SYNTHESIS AND CHARACTERIZATION OF SILVER NANOPARTICLES DEPOSITED IN TITANIUM (IV) OXIDE AS A VISIBLE LIGHT PHOTOCATALYST

[1]Arthur Ekpekpo and [2]Yalaju, Alexander Toritseju

1 &2 are of the Department of Physics, Delta stateUniversity Abraka.

ABSTRACT: *The aim of this work is to synthesis and characterizes plasmonic photocatalyst. Plasmonic photocatalyst are promising technology for high-performance photocatalysis owing to the localized surface plasmon resonance (LSPR) of the plasmonic material. This study is therefore designed to incorporate plasmonic silver nanoparticles (AgNPs) on the TiO_2 photocatalyst to improve the photo-response of the material. Plasmonic silver nanoparticles (AgNPs) was incorporated on screen-printed TiO_2 using successive ionic layer adsorption and reaction (SILAR) technique with 0, 5, 8, 11, 14, and 17 SILAR cycles. The thickness, morphological and photo-response characteristics of the Ag-incorporated TiO_2 photocatalyst were investigated using surface profilelometry, scanning electron microscope (SEM) and UV-Visible spectroscopy respectively. The thickness of the films increases with the increase in SILAR cycles. The scanning electron microscope (SEM) images reveal varied particle size distribution of the silver nanoparticles (AgNPs). Pure TiO_2 film showed a homogenous film surface while Ag-incorporated TiO_2 indicated sparkling nanoparticles with different sizes which confirms the presence of the silver nanoparticles (AgNPs). For Ag nanoparticles films on ordinary glass substrate, , the absorption peaks were observed at 439, 444, 466, 450, and 510 nm for 5, 8, 11, 14 and 17 SILAR cycles respectively. The material strongly absorbed light in the near UV and visible region but poor at the infrared region. There was a shift in the absorption towards longer wavelength when the SILAR cycles increased. At the same time, the optical bandgap of the films decreased as the SILAR cycles increased and extinction coefficient of the films also increased with the increase in the SILAR cycles. And for the Ag-incorporated TiO_2, the optical absorption edges of Ag-incorporated TiO_2 exhibit a remarkable redshift to the visible range when compared with the absorption edge of pure TiO_2 (391 nm). The material showed an optical absorption improvement over the pure TiO_2 with continuous and stronger absorption band in the visible range which can be attributed to the surface plasmon resonance (SPR) of Ag nanoparticles. Thus, the study has shown that the plasmonic photocatalyst has very efficient light absorption capability and great potential for improving many of the intrinsic limitations of conventional semiconductor photocatalysts.*

KEYWORD: Silver Nanoparticles, plasmonic photocatalyst, Titanium (IV) Oxide.

INTRODUCTION

The field of nanotechnology is rapidly growing by producing nanoproducts and nanoparticles (NPs) that can have novel and size-related physico-chemical properties differing significantly from larger matter (Tran *et al.,* 2013). The novel properties of nanoparticles have been exploited in a wide range of potential applications in medicine, cosmetics, renewable energies, environmental remediation and biomedical devices (Chaudhuri and Paria, 2012; Tran *et al.,* 2013). Among them, silver nanoparticles (Ag-NPs or nanosilver) have attracted increasing interest due to their unique physical, chemical and biological properties compared to their macro-scaled counterparts (Sharma *et al.,* 2009). Ag-NPs have distinctive physico-chemical properties, including a high electrical and thermal conductivity, surface-enhanced Raman scattering, chemical stability, catalytic activity and non-linear optical behaviour. These properties make them of potential value in inks, microelectronics, medical imaging and photovoltaic devices (Tran *et al.,* 2013; Schneid *et al.,* 2015).

Moreover, nanosilver exhibits broad spectrum bactericidal and fungicidal activity that has made them extremely popular in a diverse range of consumer products, including plastics, soaps, pastes, food and textiles, increasing their market value (Yu and Liu, 2015). To date, nanosilver technologies have appeared in a variety of manufacturing processes and end products. Nanosilver can be used in a liquid form, such as a colloid (coating and spray) or contained within a shampoo (liquid) and can also appear embedded in a solid such as a polymer master batch or be suspended in a bar of soap (solid). Nanosilver can also be utilized either in the textile industry by incorporating it into the fiber (spun) or employed in filtration membranes of water purification systems (Tran *et al.,* 2013).

On the other hand, titanium (IV) oxide (TiO_2) is one of the most promising photocatalytic materials due to its properties of chemical inertness, non-toxicity, high efficiency, long-term stability and relatively low cost (Grabowska *et al.,* 2009; Zhang *et al.,* 2012). TiO_2 has attracted lots of attention owing to its practical applications extending from common products (paints, cosmetics, toothpaste etc.) to the advanced technological applications such as photovoltaics, photocatalytic degradation of pollutants, water and air purification, optical coatings, dielectric films for new generation field effect transistors, bio-sensing and bactericidal action (Jiang, *et al.,* 2018; Zhang *et al.,* 2012; Mulmi *et al.,* 2016; Bedikyan *et al.,* 2013).

Moreover, TiO_2 is a major actor in the emerging field of oxide electronics and is regarded as the most efficient and environment friendly photocatalyst but its application suffers some limitations such as UV activation requirements due its large bandgap (3.2 eV) and recombination of photogenerated charge carriers (electrons and holes whose recombination are usually very quick). However, TiO_2 with a broad optical band gap (Eg ~ 3.20 eV) can only absorb UV light, which greatly limits its application and overall efficiency under sunlight (Wang *et al.,* 2015). Because in solar spectrum, UV light can only occupy less than 5% of total solar energy meaning that the band gap of TiO_2 (3.2 eV) is such that only UV light (≤387 nm) provides sufficient energy for the electron transfer to the conduction band (Jiang *et al.,* 2018; An *et al.,* 2017). Additionally, the fast recombination rate of photoinduced electrons (e^-) and holes (h^+), and the low quantum

efficiency are not satisfactory i. e. electron-hole charge recombination is a major weakness as it reduces the overall quantum efficiency most especially in oxide electronics and photovoltaic technology (Stucchi *et al.,* 2018; Conceic *et al.,* 2018; Shao *et al.,* 2017). Therefore, it is critical to enhance the photoresponse of titanium dioxide to the visible light region.

Numerous strategies, such as doping, semiconductor composites, and surface complexation, have been proposed to solve the issues associated with TiO_2 (Kulmas, *et al.,* 2016; Nakada *et al.,* 2017), which could expand its optical absorption range to visible light or near-infrared region and promotethe separation and transmission of photoinduced electronsand holes for improving photocatalytic efficiency (Jiang *et al.,* 2018). Among various strategies, doping with nonmetal elements, metal elements, and self-doping are considered as simple and feasible methods (Jiang *et al.,* 2018). Recently, researchers have reported that noble metal nanoparticles (NPs), such as Au, Cu, and Ag could show intense UV–Vis absorbance ability owing to their surface plasmon resonance (SPR) effect (Jiang *et al.,* 2018). Among these metals, Ag is considered as the most popular candidate due to its lower cost than that of Au, the higher stability contrast with Cu, and easier to be prepared (Yan *et al.,* 2016). For this reason, a large number of efforts have been explored to prepared Ag-based plasmon materials due to the surface plasmon resonance (SPR) effect, which could promote charge separation, improve the visible light photoresponse and develop visible-light-driven photocatalyst.

The applications of silver nanoparticles (AgNPs) combined with TiO_2 especially in photovoltaics are possible due to the metal nanoparticles small size for strong absorption and scattering of radiation in the visible region, which imparts unique properties such as absorption plasmon resonance band and high surface area as a result of localized Surface Plasmon Resonance (SPR) effects (Schneid *et al.,* 2015; Cozzoli *et al.,* 2003). The ability to synthesize noble metal nanoparticles (NPs) has drawn a considerable attention to their unique mechanical, electrical, optical, catalytic and magnetic properties due to their size-shape dependent properties and quantum size effects (Amiri *et al.,* 2015). Several forms for the preparation of metal nanoparticles films on solid substrates have already been reported, such as, vapour-deposition methods, sol-gel deposition of metal ions followed by thermal treatment and also, the deposition of metal nanoparticles from colloidal dispersions (Schneid *et al.,* 2015).

Successive Ion Layer Adsorption and Reaction (SILAR) has become a common approach to synthesizing metal chalcogenide semiconductor quantum dots. The approach, as the name suggests, involves submerging substrates in an alternating fashion into solutions containing cation and anion precursors. The absence of stabilizing ligands eliminates the need for long adsorption/chemisorption steps necessary for colloidal quantum dot deposition, and renders the particle surface free to interact chemically and electronically with the local environment (Stamplecoskie and Manser, 2014).

Objective of the Study
The aim of the research is to synthesize plasmonic silver nanoparticles (AgNPs) using successive ionic layer adsorption and reaction (SILAR) technique on the mesoporous TiO_2 with the view to

study the effects of the AgNPs on the photo-response of the TiO_2 and determine its suitability for different applications.

MATERIALS AND METHOD

Materials
The materials used for this study includes, standard laboratory 250 ml beakers, chemical reactants of analytical grade, reactants; nanostructured TiO_2 (Ti-Nanoxide T300/SP by Solaronix) semiconductor photocatalyst, silver nitrate ($AgNO_3$) (BDH) and ammonium solution (NH_3OH) (*ca.* 33 %wt NH), stannous chloride ($SnCl_2.2H_2O$) (BDH), (Grifflin and George), hydrochloric acid (HCl) (36%) (Loba Chemie) and distilled water for rinsing.

Methods

Synthesis of AG-Incorporated TiO_2 Photocatalyst

Preparation of the Substrate
Glass substrates with the dimension 75 mm x 25 mm x 1.0 mm (size of a standard microscope glass slides) were used for the thin film deposition. The glass substrates were degreased and washed ultrasonically in cleaning solution containing sodium lauryl sulphate (SLS) detergent, rinsed with distilled water. Finally, the glass slide was ultrasonically cleaned in methanol then dried in oven for 30 min at 60 ^{o}C before deposition.

Deposition of Nanostructured TiO_2
A layer of mesoporous TiO_2 (m-TiO_2) thin film was screen-printed on a selected area 25 mm x 25 mm of glass substrates with the dimension 75 mm x 25 mm x 1.0 mm. The samples were dried at 55 ^{0}C for 30 min and then sintered at 450 ^{0}C for 30 minutes, allowed to cool down to room temperature and preserved for the deposition of Ag NPs by SILAR method.

Synthesis of Ag NPs by SILAR Method
Silver nanoparticles (AgNPs) were prepared by successive ionic layer adsorption and reaction (SILAR) method using diammine silver complex and stannous chloride as starting materials i.e. cationic and anionic precursor. The cationic precursor for the SILAR method was diammine silver complex $\left([Ag(NH_3)_2]^+_{(aq)} \right)$ solution. This solution was prepared using 0.35g of $AgNO_3$ in 200ml of distilled water, to this, ammonia solution (NH_3OH) was added dropwise until colourless solution was observed and 0.01M concentration was obtained. The anionic (reducing agent) solution was prepared by adding 2 ml of concentrated HCl to 2g of stannous chloride ($SnCl_2.2H_2O$) in 640 ml of distilled water to obtain 0.2M concentration. The deposition process is illustrated in Figure 1.
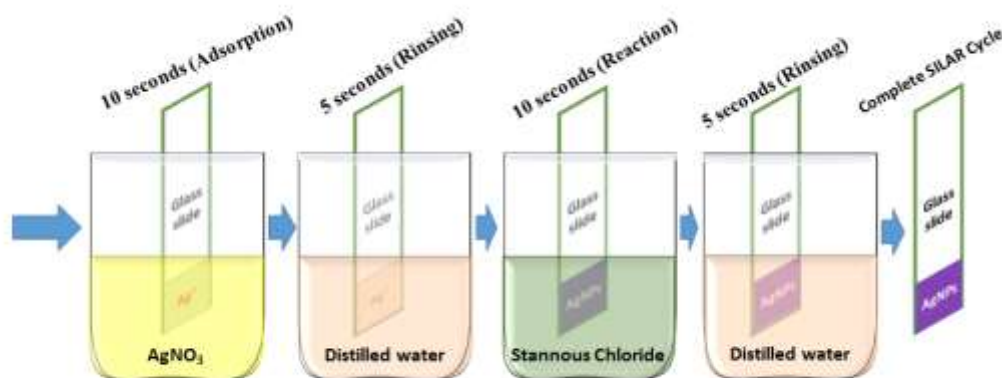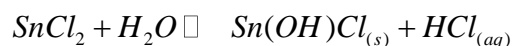
Figure 1: Scheme of SILAR cycle process of Ag nanoparticles deposition for DSSC application.
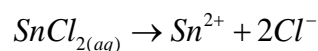
- **Anionic precursor (reaction step)**

Tin(II) chloride dissolves in less than its own mass of water to form insoluble Tin hydroxy chloride specie in a reversible hydrolysis,

$$SnCl_2 + H_2O \ \square \quad Sn(OH)Cl_{(s)} + HCl_{(aq)}$$

a clear solution of $SnCl_{2(aq)}$ requires addition of excess HCl thus;

$$Sn(OH)Cl_{(s)} + HCl_{(aq)} = SnCl_{2(aq)} + 2H_2O$$

Where

$$SnCl_{2(aq)} \rightarrow Sn^{2+} + 2Cl^-$$
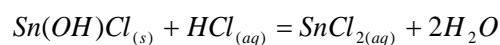
Characterization of the AG-Incorporated TiO₂ Photocatalyst

Characterisation of the films was performed to understand the optical properties and morphology of the films.

Optical absorption spectroscopy

In this work, UV/Vis Spectrophotometer (UV752N, Axiom) was used to study the spectral response of the material. UV-Vis absorption spectroscopy provides key information about the electronic transitions and hence the band gap of the material. The absorption coefficient (α), band gap (E_g) and extinction coefficient (k) of the films were evaluated from absorbance as thus:
The absorbance coefficient ($\propto$) is calculated using the equation:

$$\propto = \frac{203 \times A}{d}$$

where d is the film thickness and *A* is absorbance of the film.

Scanning Electron Microscopy (SEM)
Scanning electron microscopy (SEM) is a method for high-resolution imaging of surfaces. The SEM uses electrons for imaging, such as an optical microscope uses visible light. The advantages of SEM over light microscopy include much higher magnification (>x1,00,000) and greater depth of field up to 100 times than that of optical microscopy (Hanke, 2001).

The SEM generates a beam of electrons in an electron column above the sample chamber. The electrons are produced by a thermal emission source, such as a heated tungsten filament, or by a field emission cathode. The energy of the incident electrons can be as low as 100 eV or as high as 30 KeV depending on the evaluation objectives. The electrons are focused into a small beam by a series of electromagnetic lenses in the column. Scanning coils near the end of the column direct and position the focused beam onto the sample surface. The electron beam is scanned in a raster pattern over the surface for imaging. The beam can also be focused at a single point or scanned along a line for X-ray analysis. The beam can be focused to a final probe diameter as small as about 10 Å. In this work, scanning electron microscope (SEM) was employed to record cross-sectional micrographs of the Ag/TiO$_2$ films.

RESULTS AND DISCUSSION

Surface Profilometry of Silver Nanoparticles (AG NPs) Thin Film
The surface profilometry was performed on the films to determine their thickness value. using stylus surface Profilometer. The obtained thicknesses of the silver nanoparticles (Ag NPs) thin films deposited by SILAR method on soda lime glass substrate is presented in Table 1.

Table 1: Thickness of the as-deposited Ag NPs thin films

S/No	Number of cycles	Thickness (nm)
1	5	204
2	8	411
3	11	584
4	14	980
5	17	1340

It is observed from Table 4.1 that the thickness of the films increases with the increase in SILAR cycles.

Morphological Study of AG-Incorporated TiO$_2$ Photocatalyst
SEM images of the pure TiO$_2$ and the Ag nanoparticles incorporated TiO$_2$ photocatalyst films with different SILAR cycles are presented in Figure 2 to 8 The SEM images reveal a random two dimensional array of Ag NPs with varied particle size distribution. Figure 2 pure-TiO$_2$ while Figures 3 to 8 present SEM images of Ag-incorporated TiO$_2$ films at 5, 8, 11, 14, and 17 SILAR cycles of Ag respectively.
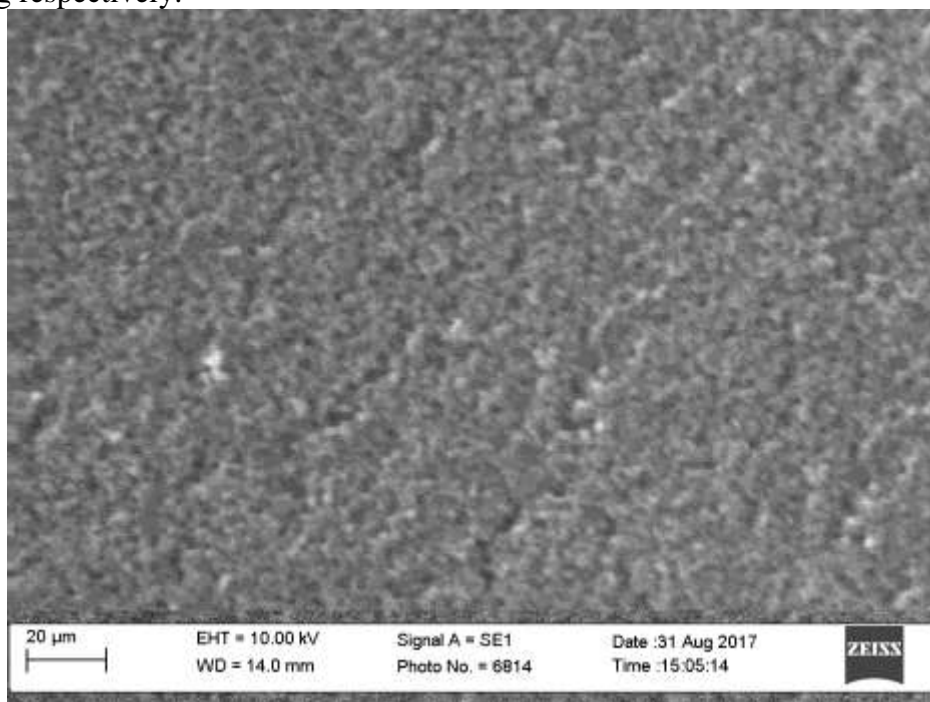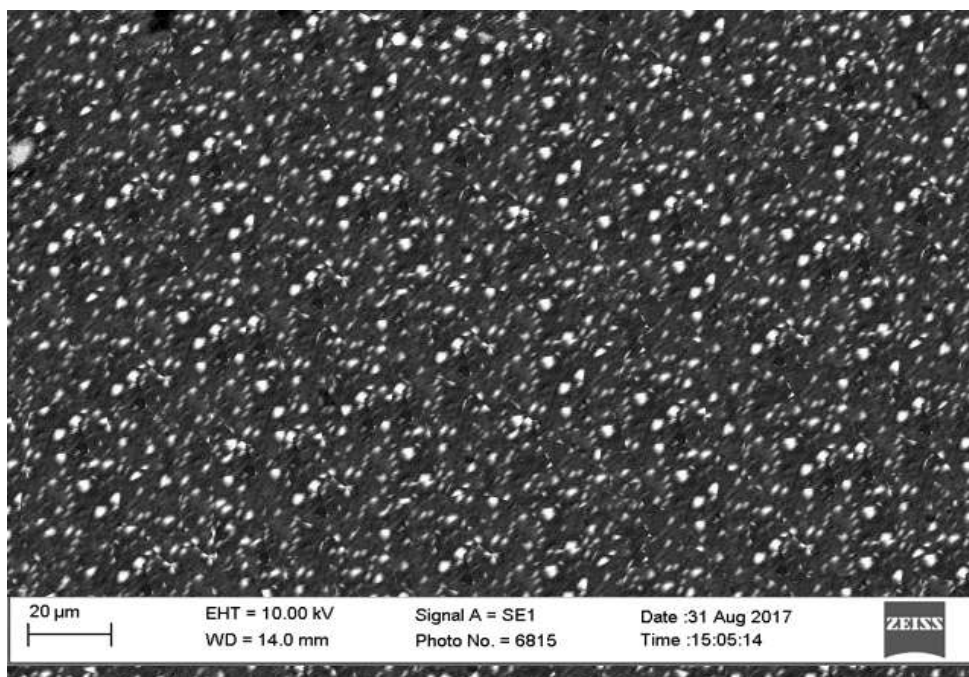

Figure 2:   SEM image of pure-TiO$_2$

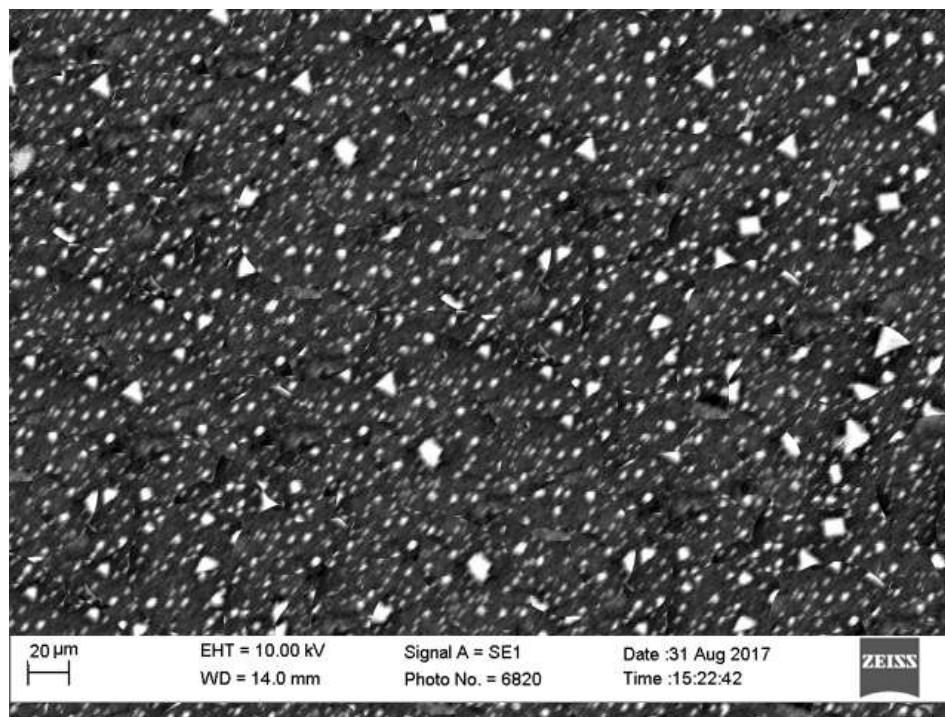**Figure 3:** SEM image of Ag-incorporated TiO_2 with 5 SILAR cycles

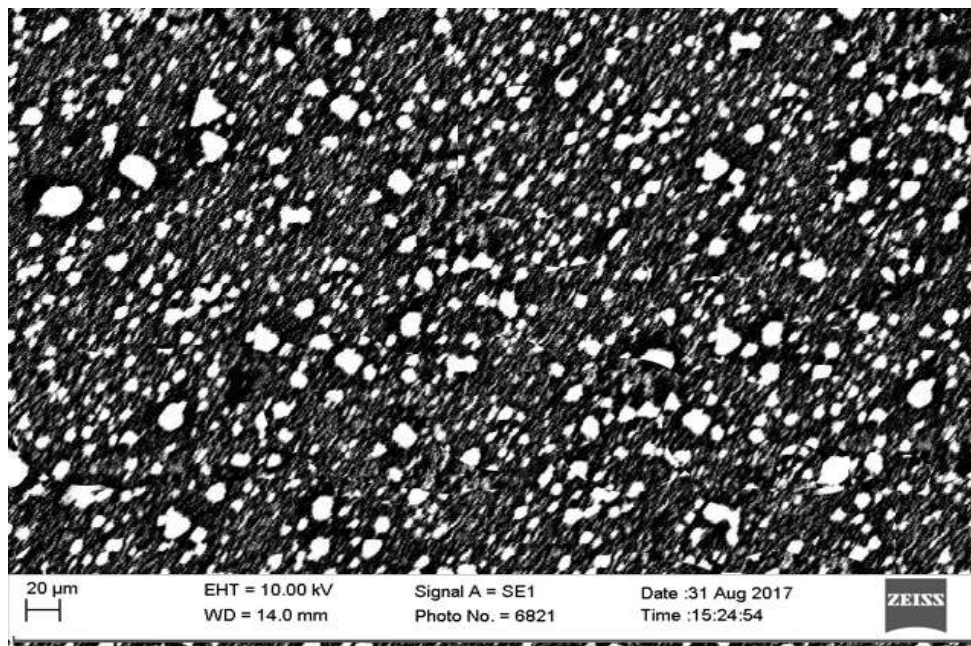**Figure 4:** SEM image of Ag-incorporated TiO_2 with 8 SILAR cycles

Figure 5:   SEM image of Ag-incorporated TiO_2 with 11 SILAR cycles
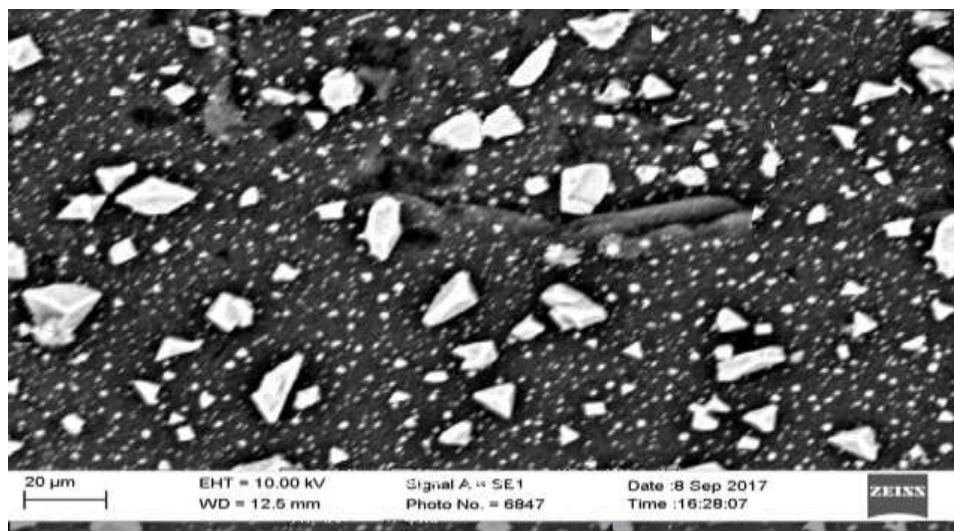

Figure 6:   SEM image of Ag-incorporated TiO_2 with 14 SILAR cycles
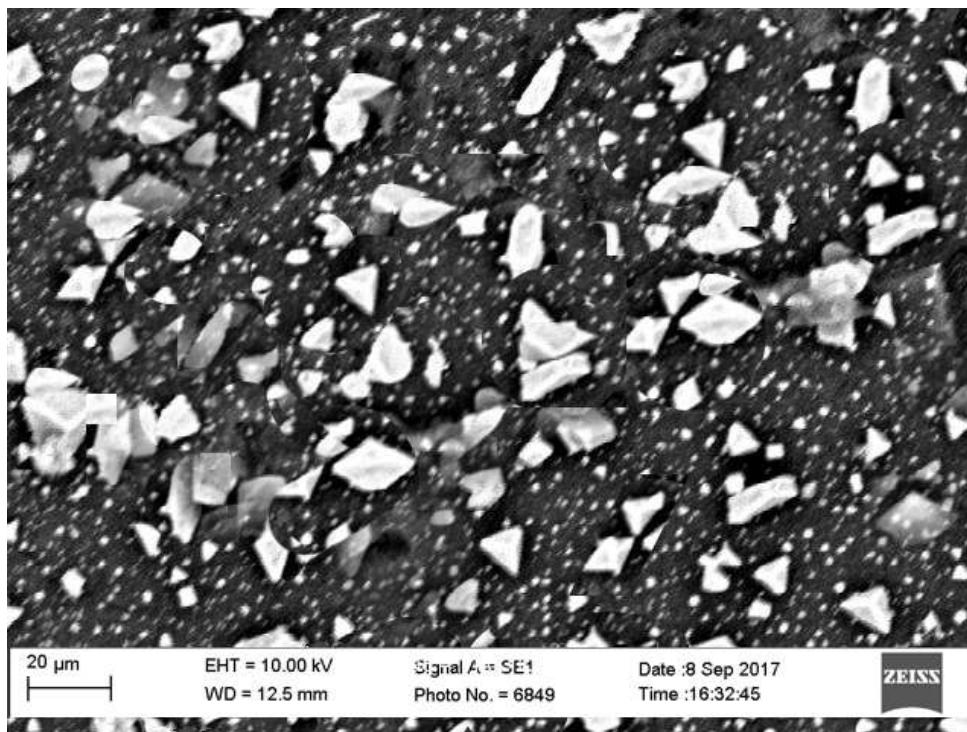
Figure 7: SEM image of Ag-incorporated TiO_2 with 17 SILAR cycles

As can be seen from Figures 2 to 7, there is variation in the images appearance. Figure 2 shows a homogenous film surface of the pure (pristine) TiO_2 and indicate absence of foreign material. As for the Ag incorporated TiO_2 indicated in Figures 3 to 7, the figures reveal the incorporation of foreign material (silver nanoparticles), which appear very sparkling (glittering) with different particle sizes as compared with SEM micrograph of pure TiO_2 in Figure 2. Considering heavy elements like Ag, they backscatter electrons more strongly than light elements like O and Ti (Yu *et al.,* 2011), so the metallic silver appears brighter in the image as observed in Figures 3 to 7. At 5 SILAR cycles, the sparkling Ag nanoparticles are well dispersed with small Ag nanoparticles and uniformly distributed as shown in Figure 3. Conversely, for a higher SILAR deposition cycles of silver, the sizes of the silver nanoparticles appear bigger as the SILAR cycles increase. It is observed that as the SILAR cycles increase, the particles come together and gradually aggregate to form bigger Ag NPs; the coalescence became obvious at 11 cycles (Figure 5) and this continued till 17 cycles.

Optical Characteristics of AG Nanoparticles

Optical Absorption of Silver NPs
The optical absorbance characteristics of the SILAR prepared silver nanoparticles films on glass substrate at 5, 8, 11, 14 and 17 cycles were investigated and the results are presented in Figures 8.
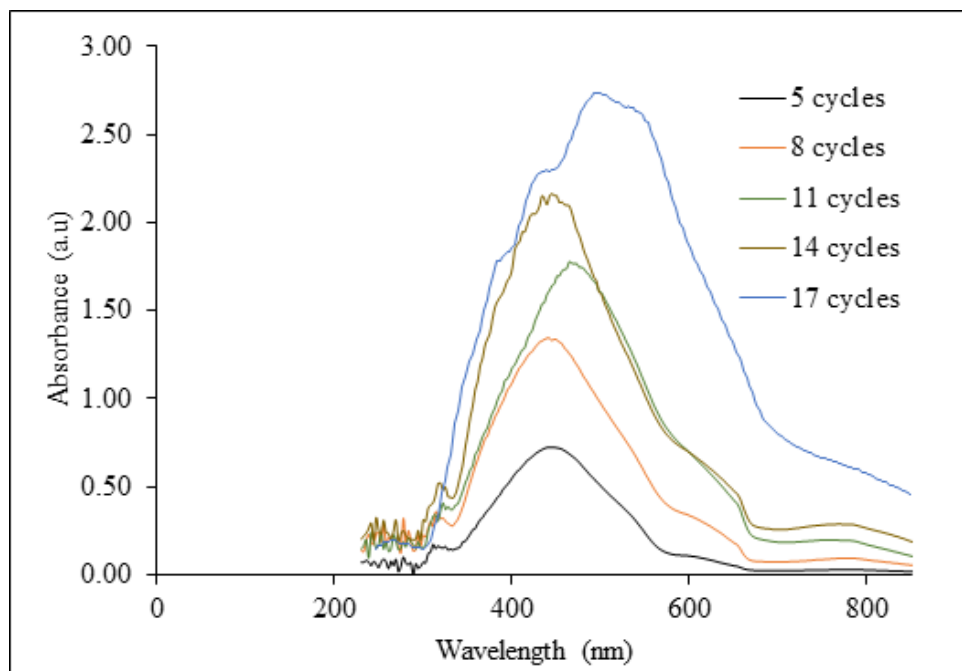
Figure 8:   Absorption spectra of silver nanoparticles synthesised at different SILAR cycles of 5, 8, 11, 14 and 17 cycles

As can be seen in Figure 8, the absorption peaks were observed at 439, 444, 466, 450, and 510 nm for 5, 8, 11, 14 and 17 SILAR cycles respectively. It is observed that the absorption continuously shifts towards the longer wavelength from 439 to 510 nm when increasing the amount of the silver on glass substrate by increasing the SILAR cycles from 5 through 17 cycles. This happens when the wavelength of the incident light matches with the oscillating frequency of the conduction electron, a surface plasmon resonance occurs, this gives rise to the absorption band in the visible region. This surface plasmon resonance peak depends on the particle size, shape, surface charge, separation between the particle and the nature of the environment (Isah *et al.,* 2016). So, the sift could be attributed to the aggregation forms as the numbers of cycles increases leading to bigger particles (Ramchiary, 2016; Isah *et al.,* 2016). These absorption peaks have been noted to correspond to a peculiar characteristic of the silver nanoparticles surface plasmon resonance band (Liu *et al.,* 2013; Ramchiary, 2016). This observation has indicated that the material has the potential to enhance a large bandgap semiconductor in the visible region.

Optical Bandgap
The optical band gap of the silver nanoparticles on glass substrate is calculated by using Tuac relation. Figure 9 shows the variation of $(\alpha h v)^{1/2}$ as a function of photon energy (hv) for allowed indirect transition of Ag NPs at different SILAR cycles for 5, 8, 11, 14, and 17 cycles.
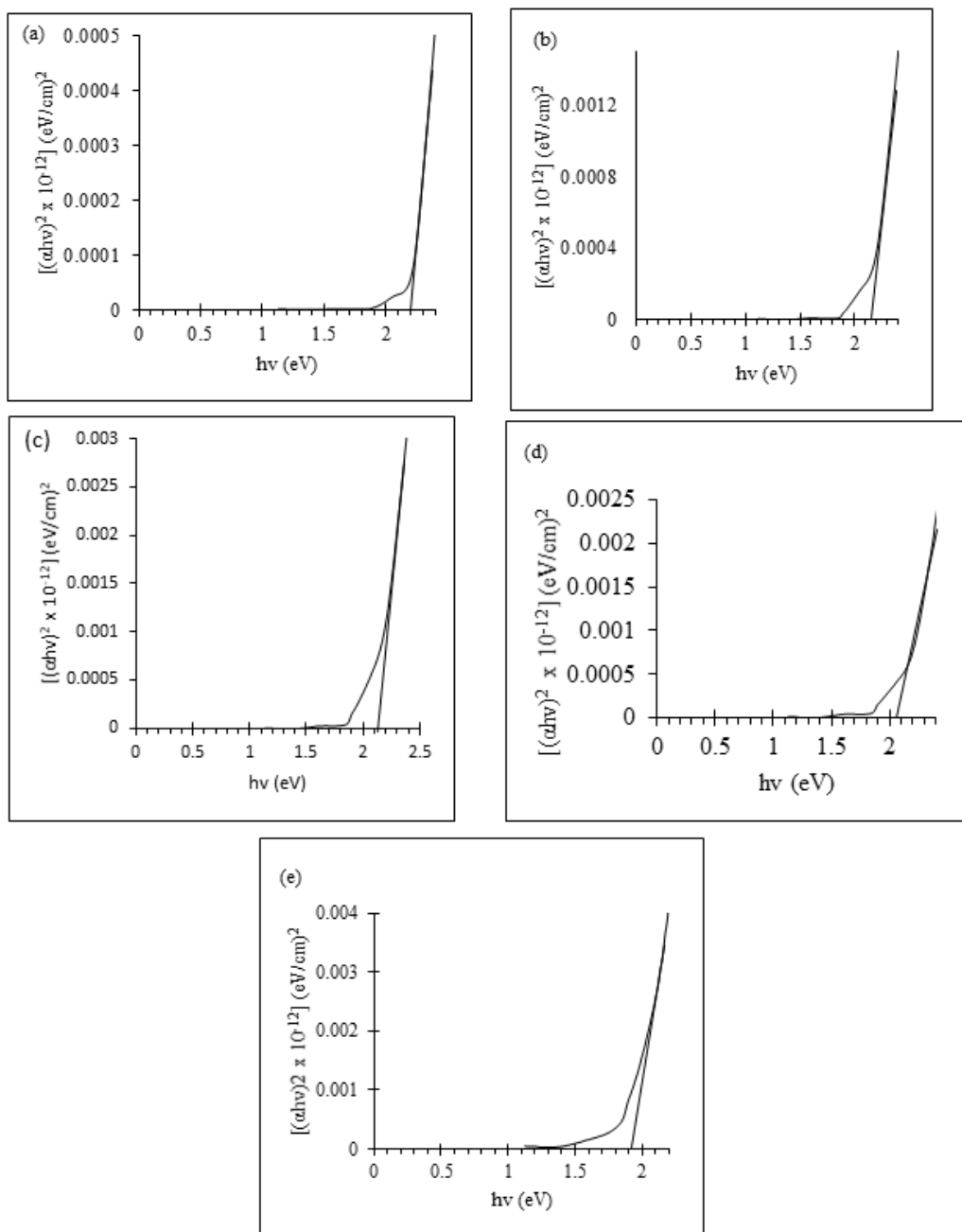
Figure 9: Determination of the optical energy band gap for AgNPs at different SILAR cycles of (a) 5, (b) 8, (c) 11, (d) 14, and (e) 17 cycles

The films exhibit different optical energy band gaps with 2.20 eV, 2.15 eV, 2.12 eV, 2.11 eV and 1.84 eV for 5, 8, 11, 14, and 17 SILAR cycles respectively. It is obvious from 9 that by increasing the SILAR cycles, the absorption edge is red shifted towards lower energy level leading to decrease in energy bandgaps owing to bigger particle size as observed in Figures 3 to 7. This observation could be ascribed to reduction of free electrons due to the increase in LSPR and scattering effects (Isah *et al.,* 2016).

Extinction Coefficient
The extinction coefficient of light is the net effect of scattering and absorption and describes the effect of the interaction between radiation and the matter upon which it impinges (Paramelle *et al.,* 2014). The extinction coefficient spectra are shown in Figure 10.
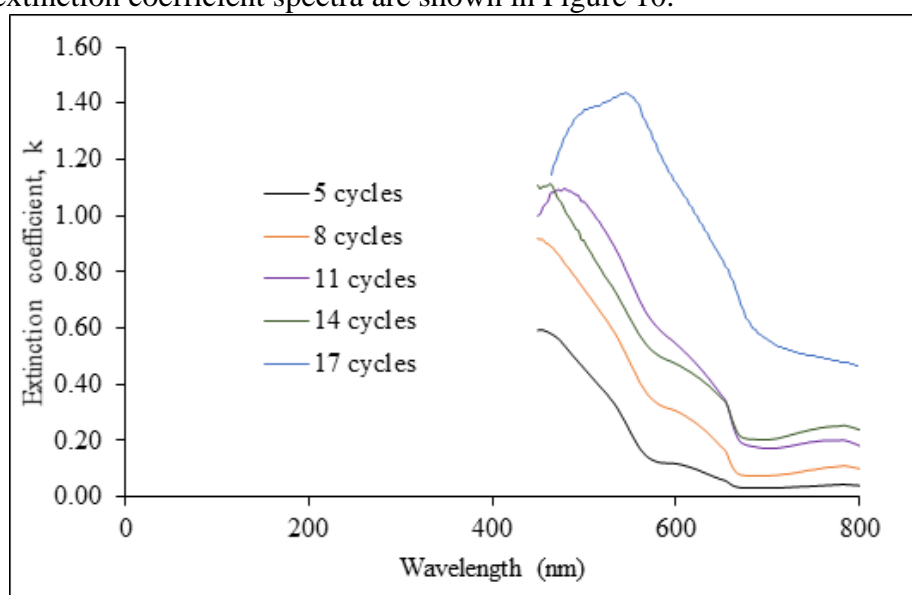

Figure 10:   Extinction spectra of AgNPs at different SILAR cycles

It is observed that the extinction coefficient increases with the increase in the SILAR cycles of silver nanoparticles which may be attributed to the contribution of the scattering effects (Paramelle *et al.,* 2014).

Optical Characteristics of Ag-incorporated TiO$_2$ Photocatalyst
The optical properties of TiO$_2$ have made this material fascinating for applications in many areas including solar cells, photocatalysis, single or multilayer optical coatings, dye-sensitized solar cells. These properties depend on its atomic distribution and can be modified/tuned by incorporating plasmonic nanoparticles. Many efforts have been attempted to enhance the charge separation efficiency and the light response and absorption of TiO2 photocalyst in the visible region by tuning of the band gap of TiO2 in order to minimise high recombination rate of charge carriers and the need for UV radiation to excite electron–hole pairs because of its large band gap (3.2 eV for anatase phase). This study incorporates Ag NPs into TiO$_2$ thin films in view to enhance

the photocatalytic properties and investigates the effect of the incorporation on the optical properties of the material.

Optical Absorption of Ag-incorporated TiO$_2$ Photocatalyst

The optical absorption characteristics of pure-TiO$_2$ and Ag-incorporated TiO$_2$ thin films are shown in Figures 11 and 12 respectively within wavelength range 300 nm - 900 nm. Figure 11 shows the variation of the light absorbance with the SILAR cycles of Ag NPs from 0 (pure TiO$_2$) to 17 cycles.
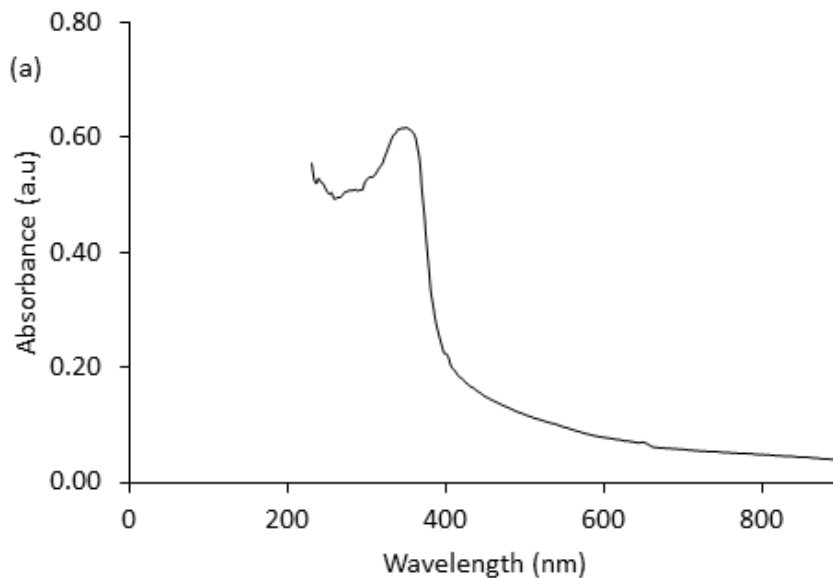

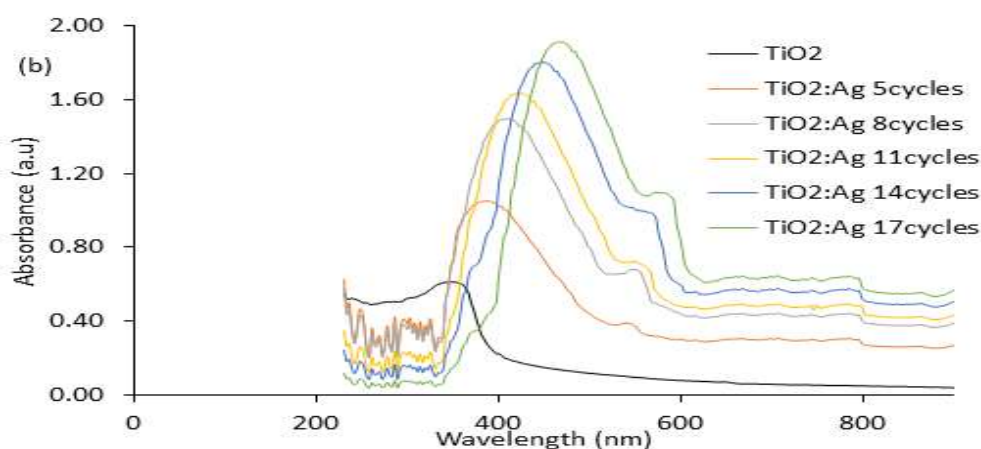**Figure 11:**   Absorption spectra of pure-TiO$_2$

Figure 12:   Absorption spectra of (a) pure-TiO$_2$ and Ag-incorporated TiO$_2$ with at 0, 5, 8, 11, 14 and 17 SILAR cycles of Ag NPs

As shown in Figure 11, the optical absorption edges of SILAR cycles of 5, 8, 11, 14 and 17 Ag-incorporated TiO_2 are 496 nm, 522 nm, 539 nm, 544 nm and 561 nm respectively, with a remarkable redshift to the visible range compared to the spectrum of pure TiO_2 (391 nm). Similarly, broad optical absorption peaks were observed around 360 nm, 386 nm, 413 nm, 419 nm, 447 nm and 472 nm for 0, 5, 8, 11, 14, and 17 cycles respectively, whereas Ag-incorporated TiO_2 films show another peaks around 560 nm in the visible region which are attributed to the surface plasmon resonance (SPR) of Ag nanoparticles (Liu *et al.,* 2013).

It can be seen that the absorption intensities corresponding to Ag-incorporated TiO_2 films are lower than the absorption intensity of pure-TiO_2 with the highest photo-response and absorption in ultraviolet region. This could be explained by the possession of Ag by TiO_2 and hence affect the intrinsic properties of the semiconductor (TiO_2 is a strong absorber of light in the ultraviolet region (Mulmi *et al.,* 2016)). The absorption intensity will reduce, when target TiO_2 samples modified by foreign substance interact with incident light in ultraviolet region. In comparison, it was observed the photo-response and absorption of the Ag-incorporated TiO_2 exhibited a higher absorption intensity than pure-TiO_2 in the visible light region. At the same time, the absorption intensity of the radiation increases when the Ag content increased from 5 to 17 SILAR cycles. This is because the silver nanoparticles incorporated into the TiO_2 has affected the dielectric constant of the surrounding matrix, thus enhancing the visible light absorption of Ag-incorporated TiO_2 films (Liu *et al.,* 2013).

Ag-incorporated TiO_2 films exhibits much continuous and stronger absorption band in the visible range, which could be attributed to the surface plasmon absorption of silver nanoparticles. Thus, due to surface plasmon resonance (SPR), the anatase Ag/TiO_2 nanoparticles shows improved photocatalytic activity under the visible light (Ramchiary, 2016). It is obvious that the Ag modification could increase effectively the absorption efficiency of TiO_2 based photocatalyst in visible light region, which is favorable to the enhancing of photocatalytic activity of TiO_2 in application of the, photovoltaics, optical coatings, dielectric films for new generation field effect transistors, photocatalytic degradation of pollutants, and waste water and air purification.

Optical Bandgap of Ag-incorporated TiO_2 Photocatalyst

The bandgap of the samples were calculated using Tauc's equation $\left(\alpha h v = A \left(h v - E_g \right)^n \right)$.

Considering TiO_2 as an indirect band gap material, its value was estimated using $\left(\alpha h v \right)^{1/2}$ vs. $h v$ plot as shown in Figure 13.
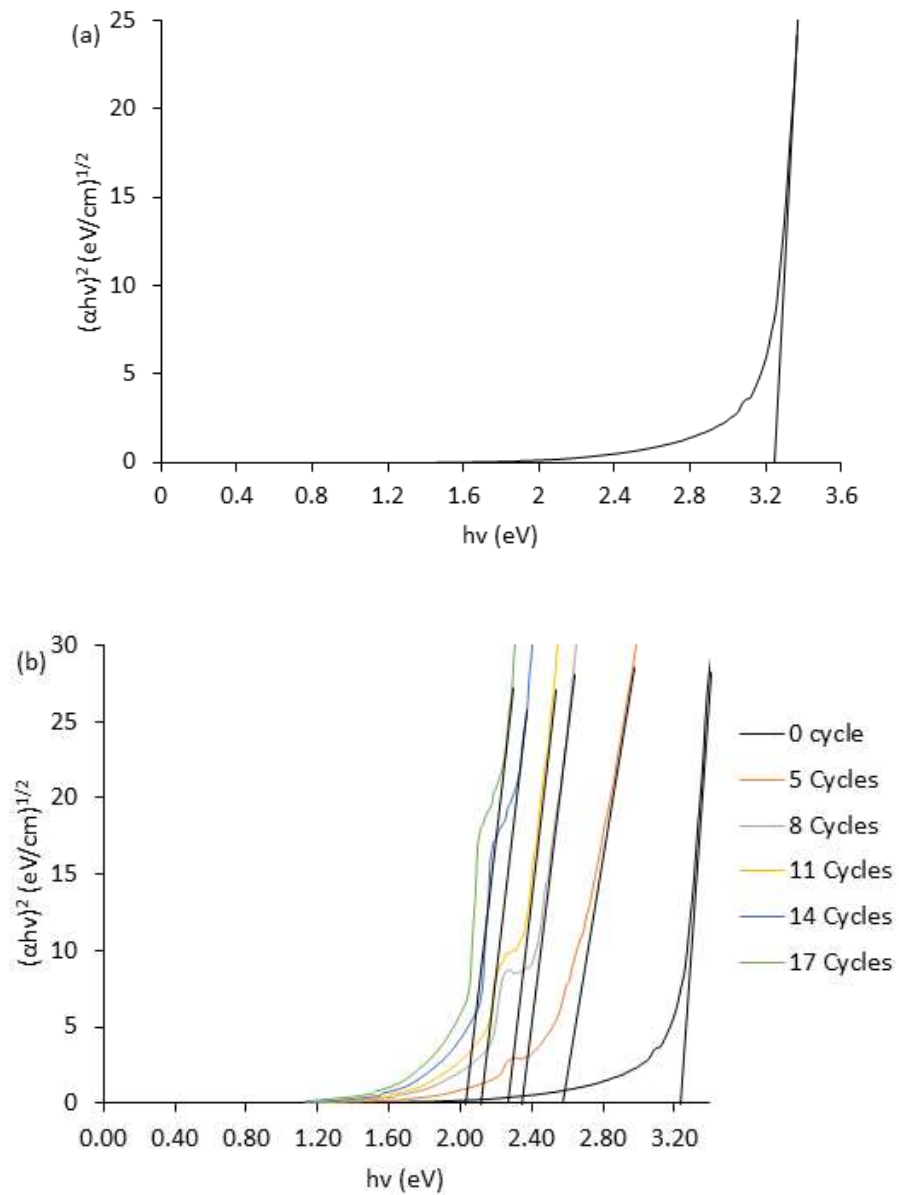
Figure 13: Tauc plots of (a) pure TiO$_2$ and (b) Ag/TiO$_2$ thin films deposited at 0, 5, 8, 11, 14, and 17 SILAR cycles of Ag.

Table 2; Estimated band gaps of different SILAR cycles

No of SILAR cycles of Ag NPs	Band gap (eV)
0	3.22
5	2.52
8	2.32
11	2.24
14	2.13
17	2.05

The band gap of pure-TiO_2 is found to 3.22eV and Ag-incorporated TiO_2 at 0, 5, 8, 11, 14, and 17 SILAR cycles of Ag are found to be 2.52 eV, 2.32 eV, 2.24 eV, 2.13 eV, and 2.05 eV, respectively as indicated in Table 2. With the incorporation of Ag nanoparticles, the band edge is marginally decreased and red-shifted, which might contribute to the enhancement of the photoactivity under visible light compared to its pristine counterpart. Hence, the reduction in the band gap of Ag-incorporated TiO_2 may be because of the creation of impurity bands inside the TiO_2 due to some diffusion of Ag particles inside the TiO_2 lattice (Zhao *et al.,* 2012; Ramchiary, 2016).

CONCLUSION

This work provides insights into the synthesis, characterization and photo-response determination of silver incorporated TiO_2 photocatalyst. A significant effort has been devoted to the development of high visible light active photocatalyst using successive ion layer adsorption and reaction (SILAR) to incorporate silver nanoparticles into the TiO_2 photocatalyst with different SILAR cycles. The results were evaluated in detail with the systematic experimentation, characterization and analysis of the photocatalysts, which fills some gaps found in the literature towards synthesis and potential applications of the photocatalyst.

The SEM images reveal varied particle size distribution of the Ag NPs. The study established that there is aggregation of the Ag NPs as the number of SILAR cycles, this is evidenced in the SEM images of Ag-incorporated TiO_2 photocatalyst. The surface plasmon resonance peak depends on the particle size, shape, surface charge, separation between the particle and the nature of the environment, tuning the size of the material could be suitably applied in many areas including solar technology to enhance light harvesting capacity and minimise carrier recombination rate (Belver *et al.,* 2015).

For the silver nanoparticles films, the material strongly absorbs in the near UV and the visible region but poor at the infrared region. There was a shift in the absorption of the silver nanoparticles

films towards longer wavelength when the SILAR cycles increased. The study could establish that the films are capable of fairly suppressing UV and visible radiations while transmitting the infrared radiations. The optical bandgap of the films decreased as the SILAR cycles increased and extinction coefficient of the films also increased with the increase in the SILAR cycles.

And for the Ag-incorporated TiO_2, the optical absorption edges of Ag-incorporated TiO_2 exhibit a remarkable redshift to the visible range when compared with the absorption edge of pure TiO_2 (391 nm). The material showed an optical absorption improvement over the pure TiO_2 with continuous and stronger absorption band in the visible range. The optical bandgap of the Ag-incorporated TiO_2 decreased as the SILAR cycles increased. Thus, the material can be employed in many areas where photocatalytic activities are desirable. Therefore, the study has shown that the plasmonic photocatalyst has very efficient light absorption capability and great potential for improving many of the intrinsic limitations of conventional semiconductor photocatalysts.

REFERENCES

Amiri, M., Nouhi, S. and Azizian-Kalandaragh, Y. (2015). Facile synthesis of silver nanostructures by using various depositionpotential and time: A nonenzymetic sensor for hydrogen peroxide. *Materials Chemzistry and Physics,* **155:** 129-135.

An, H., Park, S. Y., Huh, J. Y., Kim, H., Lee, Y. C., Lee, Y. B., and. Lee, H. U. (2017). Nanoporous hydrogenated TiO2 photocatalysts generated by underwaterdischarge plasma treatment for solar photocatalytic applications. *Applied Catalysis B,* **211**: 126–136.

Bedikyan, L., Zakhariev, S. and Zakharieva, M. (2013). Titanium Dioxide Thin Films: Preparation And Optical Properties. *Journal of Chemical Technology and Metallurgy,* **48**(6): 555-558.

Belver, C., Bedia, J. and Rodriguez, J. (2015). Zr-doped TiO2 supportedon delaminated clay materials for solar photocatalytic treatmentof emerging pollutants. *Journal of Hazardous Materials,* **322**: 233–242.

Brongersma, M. L., Halas, N. J. and Nordlander, P. (2015). Plasmon-induced hot carrier science and technology. *Nature Nanotechnology,* **10**: 25–34.

Chaudhuri, R. G and Paria, S. (2012). Core/Shell Nanoparticles: Classes, Properties, Synthesis Mechanisms, Characterization, and Applications. *Chemical Review,* **112**(4): 2373–2433.

Chen, H. M., Chen, C. K., Lin, C. C., Liu, R. S., Yang, H. S., Chang, W. S. and Tsai, D. P. (2011). Multi-bandgap-sensitized ZnO nanorod photoelectrodearrays for water splitting: an X-ray absorptionspectroscopy approach for the electronic evolution undersolar illumination. *Journal of Physical Chemistry C,* **115**:21971 -21975.

Chen, X., Zhu, H., Zhao, J., Zheng, Z. and Gao, X. (2008). Visible-Light-Driven Oxidation of Organic Contaminants in Air with Gold Nanoparticle Catalysts on Oxide Supports. *Angwandte Chemie,* **120**(9): 5433-5436.

Conceiˏ D. S. and Ferreira, L. F. (2018). Photochemical Behavior of Ag0 or Au0 Decorated Nanostructured TiO2 Prepared by a Facile In Situ Reduction Method. *ChemistrySelect,* **3***:* 773 –778.

Cozzoli, P. D., Comparelli, R., Fanizza, E., Curri, M. L. and Agostiano, A. (2003). Photocatalyticactivity of organic-capped anatase TiO2 nanocrystals in homogeneous organic solutions. *Material science and engineering C,* **23**: 707–713.

Grabowska, E., Zaleska, A., Sobczak, J. W., Gazdac, M. and Hupka, J. (2009). Boron-doped TiO2: Characteristics and photoactivity under visible light. *Procedia Chemistry,* **1**: 1553–1559.

Ha, J. W., Ruberu, T. P., Han, R., Dong, B., Vela, J. and Fang, N. (2014). Super-Resolution Mapping of Photogenerated Electron and Hole Separation in Single Metal-Semiconductor Nanocatalysts. *Journal of the American Chemical Society,* **136**: 1398–1408.

Hanke, L. D. (2001). Handbook of Analytical Methods for Materials. Plymouth: MaterialsEvaluation and Engineering Inc.

Isah, K. U., Jolayemi, B. J., Ahmadu, U., Kimpa, M. I. and Alu, N. (2016). Plasmonic effect of silver nanoparticles intercalatedinto mesoporous betalain-sensitized-TiO2 film electrodeson photovoltaic performance of dye-sensitized solar cells. *Materials for Renewable and Sustainable Energy,* **5**(10): 1-10.

Jiang, J., Xing, Z., Li, M., Li, Z., Yin, J., Kuang, J. and Zhu, W. (2018). *Journal of Colloid and Interface Science,* **521**: 102–110.

Jiang, R., Li, B., Fang, C., & Wang, J. (2014). Metal/Semiconductor Hybrid Nanostructures for Plasmon-Enhanced Applications. *Advanced Materials,* **26**: 5274–5309.

Kulmas, M., Paterson, L., Ich, K. H., Bashouti, M. Y., Wu, Y. L., Göbelt, M. and Christiansen, S. (2016). Composite nanostructures of TiO2 andZnO for water splitting application: atomic layer deposition growth anddensity functional theory investigation. *Advanced functional material,* **26**: 4882–4889.

Li, J. and Wu, N. (2015). Semiconductor-based photocatalysts and photoelectrochemical cells for solar fuel generation: a review. *Catalysis Science & Technology,* **5**: 1360-1384.

Li, J., Cushing, S. K., Meng, F., Senty, T. R., Bristow, A. D. and Wu, N. (2015). Plasmon-induced resonance energy transfer for solar energy conversion. *Nature Photonics,* **9:** 601–607.

Liu, H., Dong, X., Li, G., Su, X. and Zhu, Z. (2013). Synthesis of C, Ag co-modified TiO2 photocatalyst and its application in waste water purification. *Applied Surface Science,* **271**: 276– 283.

Lu, Z., Xu, J., Xie, X., Wang, H., Wang, C., Kwok, S.-Y. and Zhang, W. (2012). CdS/CdSe Double-Sensitized ZnO Nanocable Arrays Synthesized by Chemical Solution Method and Their Photovoltaic Applications. *The Journal of Physical Chemistry C,* **116**(4): 2656-2661.

Ma, X. C., Dai, Y. and Huang, B. B. (2014). Origin of the increased photocatalytic performance of TiO2nanocrystal composed of pure core and heavily nitrogen-doped shell: a theoreticalstudy. *ACS Applied Materials & Interfaces,* **6**: 22815–22822.

Ma, X. -C., Dai, Y., Yu, L. and Huang, B. B. (2016). Energy transfer in plasmonic photocatalytic composites. *Light: Science & Applications*, **11**:16-17.

Mulmi, D. D., Thapa, D., Dahal, B., Baral, D. and Solanki, P. R. (2016). Spectroscopic Studies of Boron Doped Titanium Dioxide Nanoparticles. *International Journal of Materials Science and Engineering,* **4**(3): 172-178.

Nakada, A., Nishioka, S., Vequizo, J. J., Muraoka, K., Kanazawa, T., Yamakata, A. and Maeda, K. (2017). Solar-driven Z-schemewater splitting using tantalum/nitrogen co-doped rutile titania nanorod as anoxygen evolution photocatalyst. *Journal of material chemistry A,* **5**:11710–11719.

Paramelle, D., Sadovoy, A., Gorelik, S., Free, P., Hobley, F. and Fernig, D. G. (2014). Rapid method to estimate the concentration ofcitrate capped silver nanoparticles from UVvisiblelight spectra. *Analyst,* **139**(1-3): 4855-4861.

Ramchiary, A. (2016). Development of structure-engineered mono/biphasic nanoscale photocatalyst systems and investigation of their solar photocatalytic activity/hydrogen. Napaam, Tezpur: Tezpur University.

Schneid, A. C., Horowitz, F., Mauler, S., Matte, C. R., Klein, M. P. and Benvenutti, E. V. (2015). Silver Nanoparticle Thin Films Deposited on Glass Surface Using an Ionic Silsesquioxane as Stabilizer and as Crosslinking Agent. *Journal of the Brazilian Chemical Society,* **26**(5): 1004-1012.

Shao, J., Sheng, W. C., Wang, M. S., Li, S. J., Chen, J. R., Zhang, Y. and Cao, S. S. (2017). In situ synthesis of carbon-doped TiO2 single-crystal nanorods with a remarkablyphotocatalytic efficiency. *Applied Catalysis B,* **209**: 311–319.

Sharma, V. K., Yngard, R. A. and Lin, Y. (2009). Silver nanoparticles: green synthesis and their antimicrobial activities. *Advances in Colloid and Interface Science,* **145**(1-2): 83-96.

Stamplecoskie, K. G. and Manser, J. S. (2014). Facile SILAR Approach to Air-Stable Naked Silver and Gold Nanoparticles Supported by Alumina. *ACS Applied Materials & Interfaces,* **6**(20):17489-17495.

Stucchi, M., Bianchi, C. L., Argirusis, C., Pifferi, V., Neppolian, B., Cerrato, G. and Boffito, D. C. (2018). Ultrasound assisted synthesis of Ag-decorated TiO2 active in visible light. *Ultrasonics - Sonochemistry,* **40**: 282–288.

Sun, S., Wang, W., Zhang, L., Shang, M. and Wang, L. (2009). Ag@Ccore/shell nanocomposite as a highly efficient plasmonicphotocatalyst. *Catalysis Communications,* **11**(4): 290-293.

Tian, Y. and Tatsuma, T. (2004). Plasmon-induced photoelectrochemistry at metal nanoparticles supported on nanoporous TiO2. *Chemical Communications,* **16**: 1810-1811.

Tian, Y. and Tatsuma, T. (2005). Mechanisms and Applications of Plasmon-Induced Charge Separation at TiO2 Films Loaded with Gold Nanoparticles. *Journal of the American Chemical Society,* **127**(20): 7632–7637.

Tran, Q. H., Nguyen, V. Q. and Le, A. T. (2013). Silver nanoparticles: synthesis, properties, toxicology, applications and perspectives. *Advances in natural sciences: nanoscience and nanotechnology,* **4**(033001): 1-20.

Wang, M. G., Hu, Y. M., Han, J., Guo, R., Xiong, H. X. and Yin, Y. D. (2015). TiO2/NiO hybridshells: p-n junction photocatalysts with enhanced activity under visible light. *Journal of material chemistry A,* **3**:20727–20735.

Wang, P., Huang, B., Dai, Y. and Whangbo, M. H. (2012). Plasmonic photocatalysts: harvesting visible light with noble metal nanoparticles. *Physical Chemistry Chemical Physics,* **14**(28): 9813-9825.

Wu, N. (2018). Plasmonic Metal-Semiconductor Photocatalysts andPhotoelectrochemical Cells: A Review. *Nanoscale,* **10**(6): 2679-2696 .

Yan, D. J., Zhu, X. D., Wang, K. X., Gao, X. T., Feng, Y. J., Sun, K. N. and Liu, Y. T. (2016). Facile andelegant self-organization of Ag nanoparticles and TiO2 nanorods on V2O5nanosheets as a superior cathode material for lithium-ion batteries. *Journal of Material Chemistry A ,* **4**: 4900–4907.

Yu, S. and Liu, J. (2015). Introduction. In j. Liu, & G. Jiald, *Silver Nanoparticles in the Environment* (pp. 1-8). Verlag Berlin: Springer.

Yu, S., Kim, Y. H., Lee, S. Y., Song, H. D. and Yi, J. (2014). Hot-Electron-Transfer Enhancement for the Efficient Energy Conversion of Visible Light. *Angewandte Chemie International Edition,* **53**: 11203–11207.

Zhang, H., Chen, G. H. and Bahnemann, D. W. (2009). Photoelectrocatalytic materials for environmental applications. *Journal of Materials Chemistry,* **19**(29): 5089-5121.

Zhang, W., Yang, B. and Chen, J. (2012). Effects of Calcination Temperature on Preparation ofBoron-Doped TiO2 by Sol-GelMethod. *International Journal of Photoenergy,* **528637**:1 - 8.

Zhang, X. M., Chen, Y. L., Liu, R. S. and Tsai, D. P. (2013). Plasmonic photocatalysis. *Reports on Progress in Physics,* **76**: 46-401.

Zhao, Y., Yang, B., Xu, J., Fu, Z., Wu, M. and Li, F. (2012). Facile synthesis of Ag nanoparticles supported on TiO2 inverse opal with enhanced visible-light photocatalytic activity. *Thin Solid Films,* **520**(9): 3515-3522.